JOURNAL OF GUIDANCE, CONTROL, AND DYNAMICS
Vol. 28, No. 1, January–February 2005

Precision Tracking Control Against Dynamic Targets for High-Energy Laser Systems

Lawrence Robertson*
U.S. Air Force Research Laboratory, Kirtland Air Force Base, New Mexico 87117
Mark Balas†
University of Colorado, Boulder, Colorado 80309-0429
Charles Tipton‡
ATA, Albuquerque, New Mexico 87123
and
Kelly Hammett§
Airborne Laser System Program Office, Kirtland Air Force Base, New Mexico 87117

Precision control of a fast-steering mirror is coupled with an open-loop acquisition system to perform tracking control against a dynamic target. The integration of a high-bandwidth tracking control system with a much lower-bandwidth acquisition system is accomplished by offloading signals from the former to the latter. This technique precludes saturation of the inner loop when large-amplitude, unexpected changes occur in the target trajectory. Particular attention is given to the sensitivities of inner-loop transient response and steady-state error responses to design conditions and sample rate. Control design solutions are presented and demonstrated via experiments and simulations.

I. Introduction

TARGET tracking and trajectory estimation has long been an area of interest for civilian and military entities. Target tracking has been applied to everything from air traffic control to missile defense. Research in this area has focused on estimation methods and filter design techniques for determining the target trajectory from radar-based and target imagery data. Radar-based filter design methods include Kalman filters,[1] alpha-beta-gamma filters,[2] nonlinear Bayesian techniques,[3] and others.

A survey of ground target tracking methods is provided in Ref. 4. Imagery-based tracking, on the other hand, has focused on closed-loop tracking applications, such as stereo[5] and active tracking.[6] Crossover research between radar and image-based tracking algorithms has been very common as shown in Ref. 7.

New areas of interest, such as high-energy laser weapon testbeds, use combinations of radar-based and image-based trajectory information during different parts of the tracking control problem. Radar and image-based trajectory estimates are used in concert to track and, in some cases, to guide the munitions to the target. For example, the U.S. Air Force Research Lab Airborne Laser (ABL) Advanced Concept Testbed had aircraft telemetry available to queue and point the telescope until an active tracking control system can acquire and track the target.[8] For systems with a single active control element, the target estimation problem can be reduced to a single filter problem. Both sets of noisy data are fed into a single trajectory estimator and weighted using respective noise covariance properties of the data.[9] However, when two trajectory estimates are used in closed loop to drive different control mechanisms, where both systems can affect the track performance, problems can arise.

For the generic case examined, radar-like information is used to drive a slow-response gimbal system with limited pointing accuracy. Once within the field of view of the focal plane, the fine track target information is derived using image-based algorithms to determine the tilt error. Because of the required speed and accuracy of the tracking system, it is assumed the radar-based information is not used after initial acquisition. A fast steering mirror (FSM) is used to close an optical control loop based on this information. If the error in the target trajectory is less than the FSM range, this control architecture is sufficient and the target "hit spot" is centered on the focal plane. If, over the engagement time, the target trajectory error is greater than the range of the FSM, because of either inaccurate target information or undetected changes in the target trajectory, the FSM will quickly reach its throw limits, and track will be lost. The solution to this problem has been to feed the FSM position into the gimbal pointing control loop as an error signal, which becomes a control design problem in itself.

The key tenet of this paper is the design and implementation of a controller that correctly offloads errors from the high-bandwidth, limited-range, inner control loop, such as a FSM/tracker system, to a much slower-bandwidth, outer control loop, such as a gimbal. A limited sensor offload sample rate will also be used. Two specific control design details are encountered and addressed given this architecture: first, necessary conditions on the design of the offload controller do not necessarily ensure proper control between the two loops, and second, the limited offload sample rate can negatively influence the inner-loop transient using type-based control design schemes. The paper presents solutions to these problems and then demonstrates these solutions via simulation of models anchored to a physical system.

II. General Dynamics Models

Figure 1 shows a diagram of the problem. The truth target trajectory information $r(t)$, given in gimbal-centered azimuth-elevation coordinates, is initially differenced with the position of the gimbal $y_g(t)$ to form a gimbal pointing error $e_g(t)$. Noise inputs, such as atmospherically induced tilt $d_{\text{atm}}(t)$ (Ref. 10), are added to the gimbal pointing error to simulate path-length errors such as optical scintillation-induced tilt. Next, the information is optically reflected

Received 29 July 2003; presented as Paper 2003-5491 at the AIAA Guidance, Navigation, and Control Conference and Exhibit, Austin, TX, 11 August 2003; revision received 1 December 2003; accepted for publication 3 December 2003.

*Aerospace Engineer, 3550 Aberdeen Avenue SE. Associate Fellow AIAA.
†Professor. Fellow AIAA.
‡Senior Scientist, 1300 Britt Street SE. Member AIAA.
§Major, USAF, 330 Target Road SE. Member AIAA.

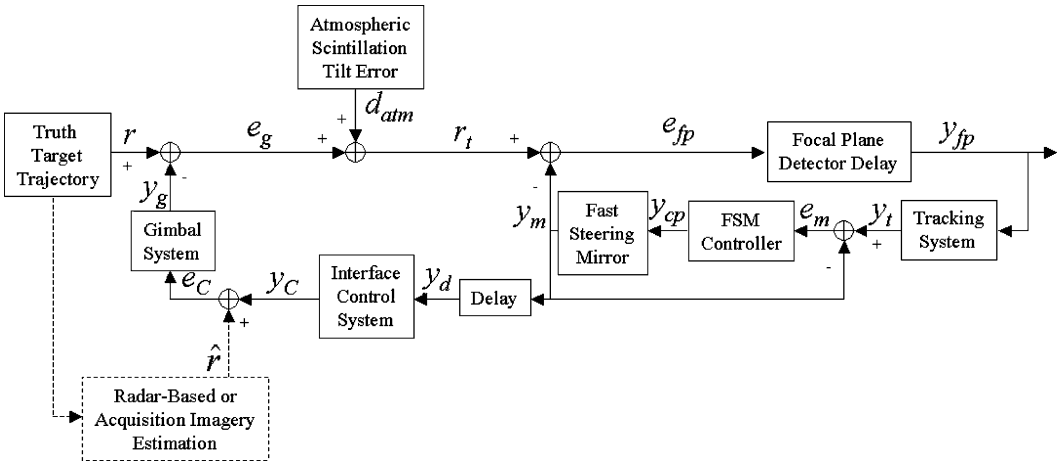

Fig. 1 Pointing and tracking control block diagram in gimbal-centered coordinates.

off of the FSM position via the subtraction of the mirror position $y_m(t)$ to form the target fine track error $e_{\text{fp}}(t)$. The FSM position is controlled via output from the image-based target estimation algorithm derived from focal plane information $y_{\text{fp}}(t)$. The target track errors from the focal plane are input to an integrator-gain controller as a command to the FSM system $y_t(t)$. There is also an analog inner FSM control loop that feeds the position of the FSM into a double lead lag and integrator controller to boost the control bandwidth. The mirror position is also sampled, shown in Fig. 1 as, $y_d(t)$ and used as an input to the interface controller $H_c(s)$. Finally, radar-derived measurements of the target trajectory $\hat{r}(t)$ are summed with the output of the interface controller $y_c(t)$ to form a command signal to the gimbal system $e_c(t)$. The main performance output of this system is the estimate of the target position via the focal plane. Errors in the estimate of the focal-plane-derived target position such as pixel quantization, focal plane noise, and inconsistencies in the track algorithm are assumed to be negligible and not included in this analysis.

Working from the innermost loop out, the FSM has its own control loop to compensate for the low-frequency response of the open-loop system. For simplicity, the FSM is modeled as

$$Y_m(s) = G_m(s)Y_{\text{cp}}(s) = \left[\omega_m^2 \Big/ \left(s^2 + 2\zeta_m\omega_m s + \omega_m^2\right)\right]Y_{\text{cp}}(s) \quad (1)$$

where ω_m is the frequency of the first mode of the mirror-flexture system, ζ_m is the damping factor of the first mode of the mirror-flexture system, $Y_m(s)$ is the mirror position from an eddy current probe, and $Y_{\text{cp}}(s)$ is the voltage input into the voice coil actuator. To compensate for the low first mode, a double-lead, integrator, gain controller of the following form is used:

$$Y_{\text{cp}}(s) = H_m(s)E_m(s) = (K_{\text{mc}}/s)[(s + z_{\text{mc}})/(s + p_{\text{mc}})]^2 E_m(s) \quad (2)$$

where z_{mc} and p_{mc} are design parameters. Outside of this loop is the focal plane and computer tracking system. Relevant dynamics include a discrete-time integrator, a focal-plane integration delay, focal-plane read-out delay and representative scale factors as shown in Eq. (3):

$$Y_T(z) = H_{\text{TR}}(z)Y_{\text{FP}}(z) = K_{\text{tr}}\left[\tau_{d_{\text{Tracker}}} \Big/ (z-1)\right](1/z)^2 Y_{\text{FP}}(z) \quad (3)$$

Using these models, the combined FSM/tracking system is eighth order given by

$$\begin{bmatrix} Y_{\text{fp}}(z) \\ Y_m(z) \end{bmatrix} = \begin{bmatrix} T_{\text{fp}}(z) \\ T_m(z) \end{bmatrix} R_T(z) \quad (4)$$

Outside of the tracking system loop are the offload controller, the mirror measurement delay, and the gimbal system. Modeling of gimbal control systems can be quite complex given the sheer number of different gimbal configurations and issues such as the 90-deg elevation singularity commonly found in elevation-over-azimuth gimbals. However, simple dynamics models can be built that capture the small angle motion dynamics. A good approximation for gimbals is

$$Y_g(s) = G_g(s)E_c(s)$$

$$= \frac{K_g}{s+p}\prod_{i=1}^{n}\left(K_i\frac{s^2 + 2\zeta_{\text{zg}_i}\omega_{\text{zg}_i}s + \omega_{\text{zg}_i}^2}{s^2 + 2\zeta_{\text{pg}_i}\omega_{\text{pg}_i}s + \omega_{\text{pg}_i}^2}\right)E_c(s) \quad (5)$$

where n is usually 1, 2, or 3 depending on the response shape. In general, most gimbals act like simple second-order systems with characteristic overshoot and ring-out step responses. However, extra pole-zero pairs might be needed to capture longer rise time system dynamics. If the ring-out contains only one frequency, the second-order poles can be very closely spaced, whereby $\omega_{\text{pg}_1} \approx \omega_{\text{pg}_2} \approx \cdots \approx \omega_{\text{pg}_n} \approx \omega_{\text{pg}}$. The same can also be true of the zeros and damping factors.

The delay between the FSM position and the control system can be modeled using simple $1/z$ discrete transfer functions or a continuous time Pade approximation of the delay given by

$$Y_d(s) = G_d(s)y_m(s) = \frac{1 - \tau_d s/2}{1 + \tau_d s/2}Y_m(s) \quad (6)$$

Given this complex plant, design of the offload controller $H_c(s)$ can be performed.

III. Controller Design

A quick examination of the problem reveals some constraints. First, the error signal $E_g(s)$ between the reference signal $R(s)$ and the gimbal position $Y_g(s)$ cannot be measured. In many disturbance rejection problems, the error signal is usually available to monitor the performance of the controller. Second, the initial reference $R(s)$ is not available either. In control design situations where the reference signal is unavailable, the problem can be restated into a class of disturbance rejection problems. Simple type tests can reveal what type of disturbances can be rejected. Finally, for this control design scheme the gimbal position $Y_g(s)$ was not used.

Using simple type-tests control design techniques, specific forms of the controller become apparent. Given that, one, the target trajectory can be written as

$$r(t) = \alpha + \beta t + \gamma t^2 = \gamma t^2 \quad (7)$$

and two, the atmospheric disturbance $D_{\text{ATM}}(s)$ is white or near white with zero mean, then to maintain track, that is, for $y_{\text{fp}}(t)$ to be zero mean, $H_c(s)$ must be designed so that the following is true:

$$\lim_{t\to\infty} y_{\text{fp}}(t) = \lim_{s\to 0} sY_{\text{fp}}(s)$$

$$= \lim_{s\to 0}\frac{s[1 - T_m(s)]}{1 + G_g(s)H_c(s)G_d(s)T_m(s)}R(s) = 0 \quad (8)$$

The goal of driving $y_{\text{fp}}(t)$ to a zero mean value is based on the desired to keep the track system aligned with the adaptive optics system in

order to minimize tilt anisoplanatism at the target.[11] For simple analysis purposes, if $\tau_{d_{\text{Tracker}}} \ll 2\pi/(\omega_m)$ then $H_{\text{TR}}(s) = K_{\text{TRs}}/s$, $T_m(s)$ is sixth order, that is,

$$T_m(s) = \frac{\omega_m^2 K_m (s + z_{\text{mc}})^2 K_{\text{TRs}}}{\left(s^2 + 2\zeta_m \omega_m s + \omega_m^2\right)(s^2)(s + p_{\text{mc}})^2 + \left[\omega_m^2 K_m (s + z_{\text{mc}})^2\right](K_{\text{TRs}} + s)} \tag{9}$$

Note that by using Eq. (9) in Eq. (8), $T_m(0) = 1$ and the limit is initially indeterminate. Using I'Hôspital's rule implies a controller of the form

$$H_c(s) = H_{c1}(s) = K(1/s^2 + 1/s) \tag{10}$$

is sufficient. Finally, given the block diagram in Fig. 1, the controller is input via

$$E_c(s) = H_c(s) Y_d(s) + \hat{R}(s) \tag{11}$$

to produce a stable tracking system. Note that if the control design and analysis is performed as a tracking problem, that is,

$$\lim_{t \to \infty} e_g(t) = \lim_{s \to 0} s E_g(s) = \lim_{s \to 0} \frac{s}{1 + G_g(s) H_c(s) G_d(s) T_m(s)} R(s) = 0 \tag{12}$$

then

$$H_c(s) = H_{c2}(s) = K(1/s^3 + 1/s^2 + 1/s) \tag{13}$$

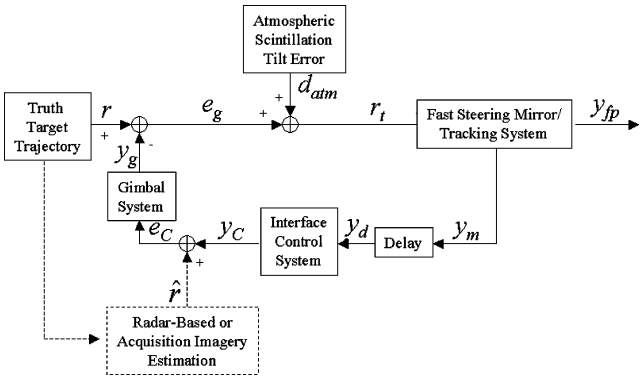

Fig. 2 Basic blocks of a pointing and tracking control diagram in gimbal-centered coordinates.

Also, note that

$$\lim_{t \to \infty} y_m(t) = \lim_{s \to 0} s Y_m(s) = \lim_{s \to 0} \frac{s T_m(s)}{1 + G_g(s) H_{c1}(s) G_d(s) T_m(s)} R(s) = K \tag{14}$$

Notice that control design via the focal plane output only guarantees a constant nonzero, steady-state mirror position. If the theoretical mirror steady-state position is greater than the actual range of the mirror, track will be lost. The tracking error rejection methodology guarantees a zero focal plane and zero-mirror-position steady-state output. It also contains an extra controller pole at the origin to meet these criteria.

A constant velocity target, that is, γ is zero and β is a constant, demonstrates the control design issue. Because β is a constant, controllers of the form

$$H_c(s) = K/s \tag{15}$$

will yield tracking results with a constant mirror position error and zero offset. A discrete time version of Eq. (15) can be written as

$$Y_c(z) = [z/(z-1)] K_D Y_D(z) \tag{16}$$

which will command the gimbal to compensate for errors in the estimate of the velocity. For this situation, the controller sample rate is matched to the delay. However, the net focal plane output result depends on the magnitude of the control commands Y_c and how those inputs are filtered through the gimbal and FSM dynamics. Large step commands to the gimbal, when filtered through the gimbal and FSM/tracking system, can cause jumps in the error that are noticeable in the track system. Because the error rejection of the FSM is finite, some offload command errors are seen at the focal plane at a frequency equal to the inverse of the delay time.

One method to mitigate this problem is to ramp the commands into the controller given by

$$\hat{Y}_M = \left[\frac{T_{s_C}}{2}\left(\frac{z+1}{z-1}\right)\right]\left[\frac{2}{T_{s_D}}\left(\frac{z-1}{z+1}\right)\right] Y_D \tag{17a}$$

$$Y_c(z) = \left(\frac{z}{z-1}\right) K_D \hat{Y}_m(z) \tag{17b}$$

where T_{S_D} is the delay sample period between the controller and the mirror position output and T_{S_C} is the sample period of the controller. This controller works by first estimating the velocity of the mirror position and then integrating that value at the fast controller speed to create a fast estimate of the mirror position. The result of that estimate is then fed to the standard integral controller found in Eq. (17b), which follows the standard final-value theorem results.

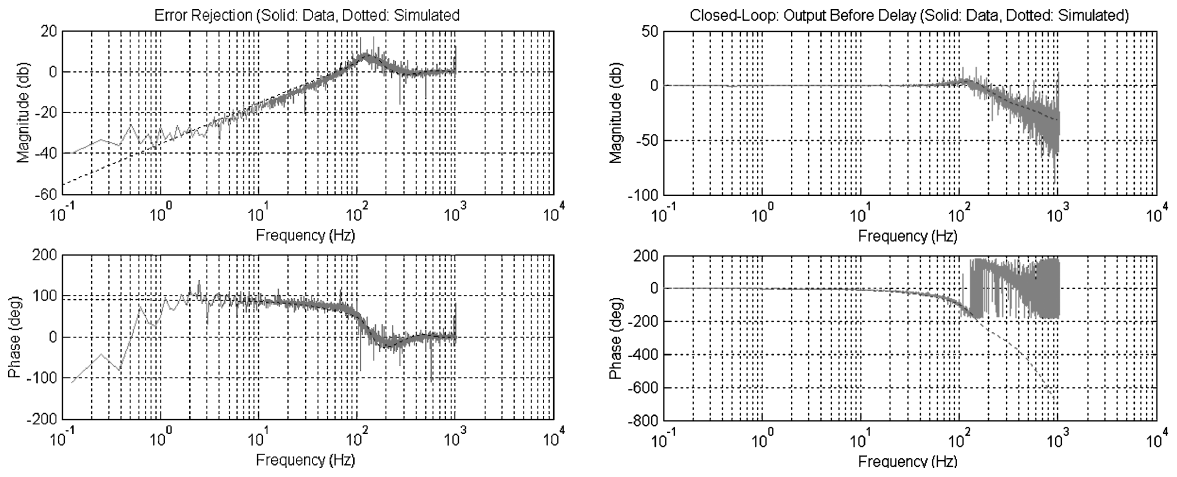

Fig. 3 FSM/tracking system model and system frequency-response plots.

A computer software interpretation of this controller is

$$Y_c(z_1+1) = (1/z)Y_c(z_1) + K_{D2}\Big\{Y_M(z_2-1) + \Big(1\Big/\Delta t_{z_2}\Big)[Y_M(z_2) - Y_M(z_2-1)]\Big(t - t_{z_2}\Big)\Big\} \quad (18)$$

where $t_{z_2} < t < t_{z_2+1}$ and the sample rate for z_1 is faster than for z_2. Both sets of controllers in Eqs. (16) and (17) were created from this analysis, whereas the controller in Eq. (18) was input into a real hardware system. This design idea works for systems of any order.

IV. Model Anchoring and Reduced-Order Models

To anchor the models developed, test data from the Air Force Research Lab Advanced Concept Testbed (ACT) were used. All output variables are in arbitrary pixel units, with some data given in microradians. However, atmospheric turbulence values, ranges to targets, and the maximum latency time of the tracking systems have not been included. Parameters such as frame rate were varied in both the model and ACT testbed to test model sensitivity. In general, frequency-response-function data were taken for the FSM system, whereas step-response data were used for the gimbal. Figure 2 shows the basic blocks developed. Details on ACT hardware can be found in Ref. 8 but are not needed to perform the simulations. Table 1 shows values used in the simulation of ACT. These values are put in terms of the rest of the variables used in the paper.

Figure 3 shows the comparison of the simulation results to the actual test results for the 5.5-in., flexture-mounted FSM and Mercury computer-based fine tracking system used on ACT. Notice that the simulation agrees quite well with the actual data, with the exception of the phase wrap in the test data that is simply an artifact of the test apparatus and is not real. The model was also found to be accurate at all focal plane integration rates. Transfer functions of each block were taken and checked at every step to arrive at the system model. Issues such as conversion factors and software gains were meticulously investigated. The model-based system was order eight and was based on using the discrete model extraction tool in MATLAB®.

For the gimbal system, a small step-motion model was developed. Figure 4 shows the raw 400 microradian azimuth step-response data used to derive the gimbal model. Raw step-response data from the ABL-ACT gimbal were input into MATLAB and a model derived from that data. Figure 4 also shows the step response of a fifth-order model. The model was built using subspace system identification methods.[12] The step response of the model matches well with the captured data. Data were also taken for a negative step with similar dynamics found compared to the positive step response. Elevation step-response data were taken but not included in the model.

After modeling the system, reduced-order models (ROMs) were created to facilitate controller design. The ROMs were not meant to be completely accurate models of the system, but more helpful at providing insight into what was needed to design the controllers.

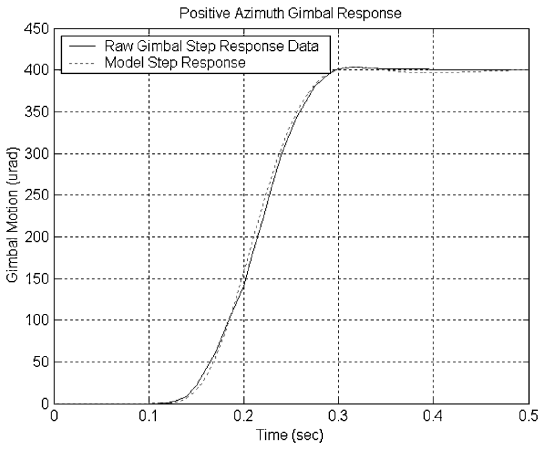

Fig. 4 Gimbal positive azimuth step response.

Table 1 Values used in simulations

Parameter	Values	Parameter explanation
ω_m	62.8319	Open-loop first FSM mode
ζ_m	0.007	Open-loop first FSM mode damping
p_{mc}	18,850	FSM control compensator pole
z_{mc}	502.6548	FSM control compensator zero
K_{mc}	166,293,339	FSM control compensator gain
K_{tr}	372.5919	Tracker gain
$\tau_{d_{\text{Tracker}}}$	$4.8591e{-}004$	Tracker sample period
p	21	Gimbal first-order pole
ω_{pg}	37.8021	Gimbal second-order pole
ζ_{pg}	0.6084	Gimbal second-order pole damping
K_g	1	Gimbal gain
ω_{zg}	(No zero/not used)	Gimbal second-order zero
ζ_{zg}	(No zero/not used)	Gimbal second-order zero damping
T_{S_D}	0.1	Mirror position sample period
T_{S_C}	0.01	Interface controller sample period
α	0	Truth target position
β	1000	Truth target velocity
γ	0	Truth target acceleration
$\hat{\alpha}$	0	Estimated target position
$\hat{\beta}$	700	Estimated target velocity
$\hat{\gamma}$	0	Estimated target acceleration
K_f	1	Reduced-order model (ROM) FSM gain
τ_f	641	ROM FSM pole
$\zeta_{\text{pg}_{\text{RO}}}$	0.8	ROM gimbal damping
$\omega_{\text{pg}_{\text{RO}}}$	18.8	ROM gimbal frequency
K_D	0.5	Interface controller gain

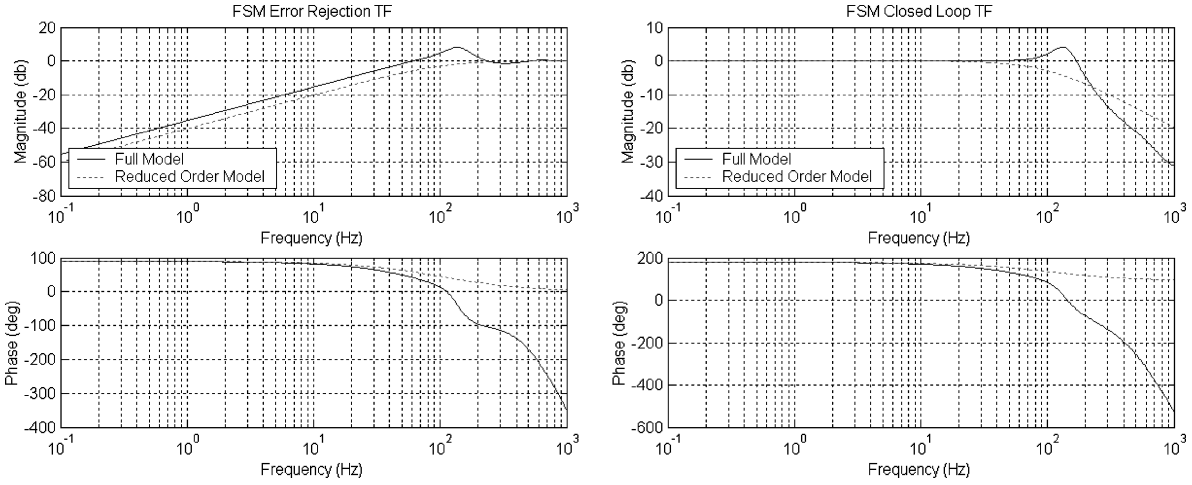

Fig. 5 Full-system model vs reduced-order model.

Any ROM-based control designs were subsequently implemented on the full model to test stability and performance. Because the ROMs were built around the idea of capturing the relevant dynamics of the system, the first modes of the larger system models were used. For the FSM/tracking system, simple transfer functions from the reference input $R_T(s)$ to the focal plane output $Y_{\text{fp}}(s)$ and the mirror position $Y_m(s)$ can be written as

$$\begin{bmatrix} Y_{\text{fp}}(s) \\ Y_m(s) \end{bmatrix} = \begin{bmatrix} T_{\text{fp}}(s) \\ T_m(s) \end{bmatrix} R_T(s) = \begin{bmatrix} \dfrac{K_f s}{\tau_f s + 1} \\ \dfrac{K_f}{\tau_f s + 1} \end{bmatrix} R_T(s) \tag{19}$$

assuming that the focal plane operates at an integration rate significantly higher than the first mode of the mirror-compensator closed-loop system. Even though the total system order is eight, most of the dynamics are beyond the focal plane integration rate. The one regret is the ROMs did not capture the underdamped behavior of the FSM/Tracking system model. The underdamped nature of $T_m(s)$ appears to be second order, but the roll off is first order in nature. For simplicity, these transfer functions capture most of the dynamics of the system. Figure 5 shows the comparison of the full model to the ROM for the atmospheric tilt error input to the mirror position transfer function.

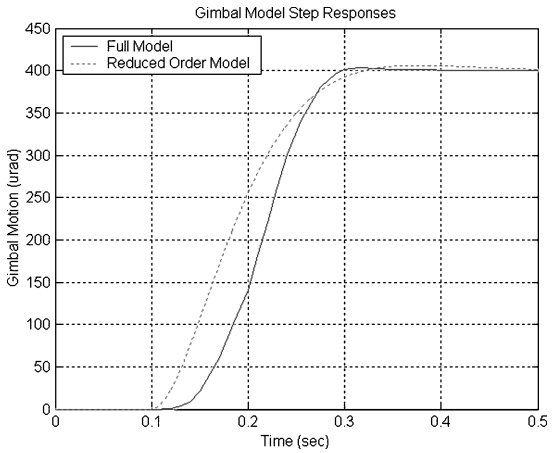

Fig. 6 Full-system model vs reduced-order model for the gimbal system.

For the gimbal, the reduced-order model problem is more complex. Reducing the order adversely affects the settling time and overshoot. However, a simple second-order model of the form

$$Y_g(s) = G_{g\text{RO}}(s) Y_c(s)$$

$$= \left[\omega_{\text{pg}_{\text{RO}}}^2 \Big/ \left(s^2 + 2\zeta_{\text{pg}_{\text{RO}}} \omega_{\text{pg}_{\text{RO}}} s + \omega_{\text{pg}_{\text{RO}}}^2 \right) \right] Y_c(s) \tag{20}$$

using only one set of modes instead of double or triple complex pole and zero pairs can be used. Figure 6 shows the step response of the actual system, the system identification comparison and the reduced-order model of order two.

V. Simulation and Experiment Results

Once the reduced-order models were built, controllers based on those models were designed. Figure 7 shows the SIMULINK version of the full-system model with the variable names used in the paper. Using the reduced-order models, a control gain K_D of 0.5 was chosen and then tested on the full-system model. Figure 8 shows the simulation results using controller (16) and (17) for the focal plane output. For the simple controller in Eq. (16), notice the steady-state

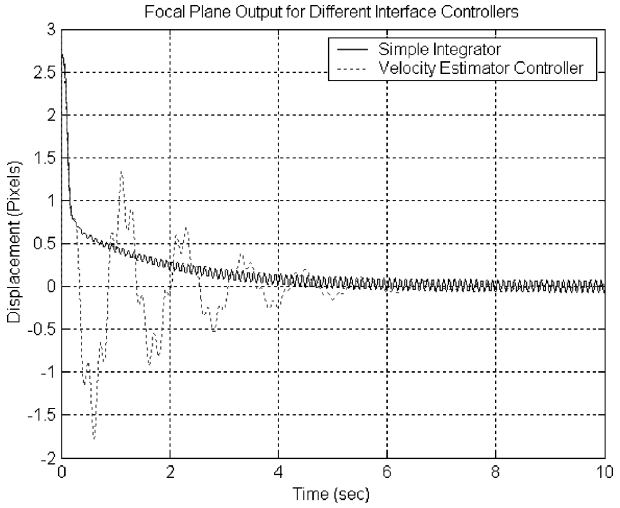

Fig. 8 Simulation results of focal plane output for different interface controllers.

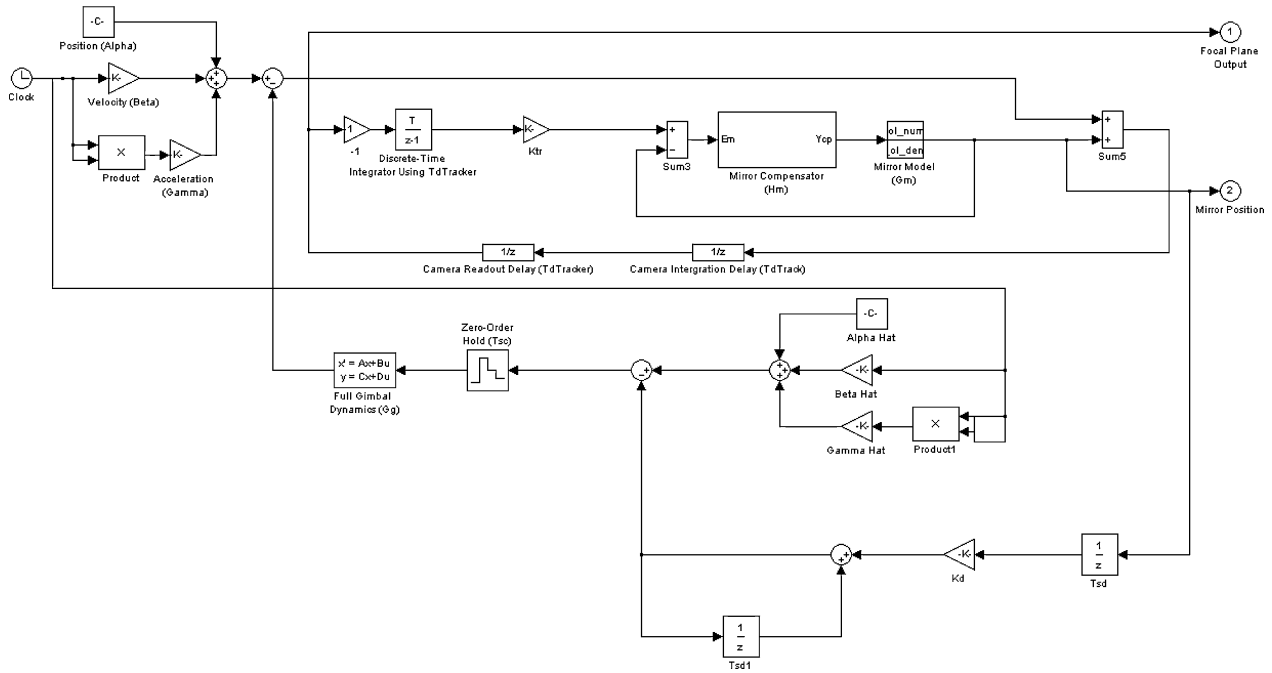

Fig. 7 SIMULINK model of the system.

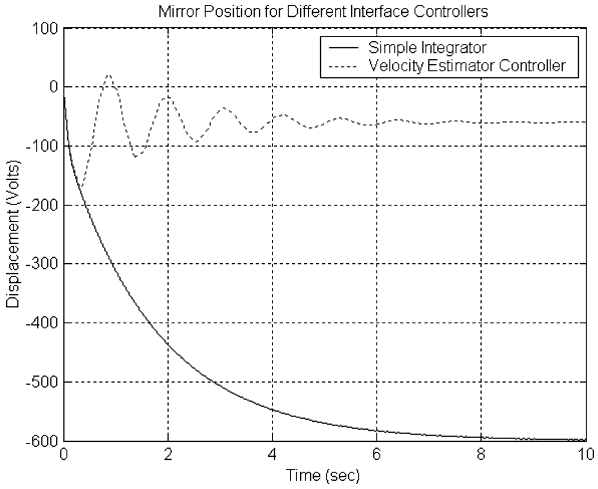

Fig. 9 Simulation results of mirror position output for different interface controllers.

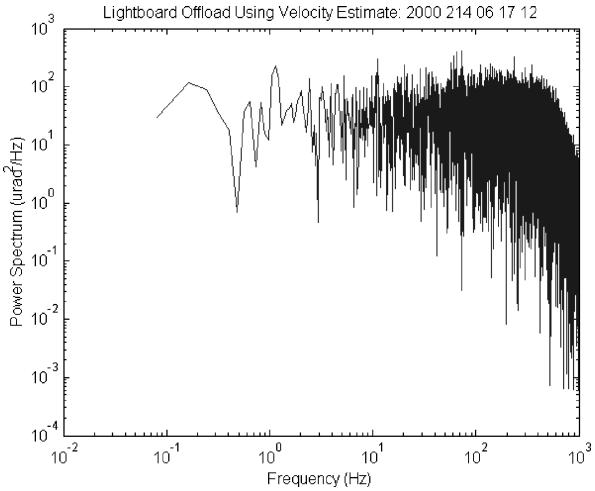

Fig. 10 PSD using velocity offload on a lightboard target.

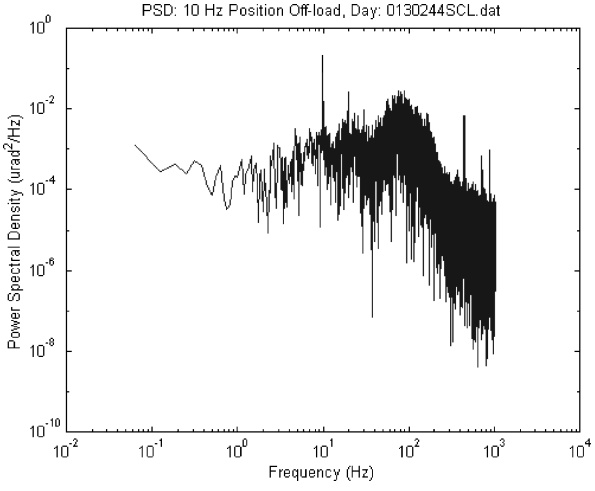

Fig. 11 PSD using integral control against a point source.

ringing at the focal plane output. The velocity estimation controller response does not contain any steady-state ringing; however, there is a significant transient response to this controller. If the response is beyond the mirror position capability, the gain will have to be lowered to compensate for this problem. Figure 9 shows the mirror position data using the two controllers. Notice how the velocity estimation controller also creates a smaller steady-state mirror position output.

Next, the controllers were implemented on the ACT system and tested. Figures 10 and 11 shows the power spectral density of the focal plane position using both the more complex controller in Eq. (17) and the simple controller from Eq. (16) respectively from different dates. The general shape of the power spectral density (PSD) is caused by atmospheric-induced scintillation, whereas the difference in the dc noise level of the tilt spectrum between the two figures, that is, the mean value of the PSD at low frequency, is caused by changes in the atmospheric-induced tilt caused by increased integrated atmospherically induced turbulence along the path to the target. However, notice the spike at 10 Hz caused by the delay in reading the mirror position in the simple controller system. Using the velocity estimation controller, the spike disappears, and the control system works normally. In general, the velocity estimation is necessary for interfacing the FSM system to the gimbal control system.

VI. Conclusions

A solution to offloading nested inner-control loop errors onto an outer-loop controller has been presented. Specifically, the major problem of a reduced sample rate offload error was overcome via design of an estimator that creates a smoothed higher-order estimate of the offload trajectory. A constant velocity target was used, but the control design conditions needed for a family of target trajectories were also discussed. The control design explored allows the large offload to be implemented onto the outer loop slowly and thus reduces the transients found on the inner-control-loop output. One degenerate control design case was also discovered, whereby type-based control design using only input and output tests do not guarantee steady-state positioning of the inner loop offload position. This result has implications when the inner-loop system might have range limitations. The implication is control design via output-only-based metrics is incomplete with error-based design necessary for correctly designing an acquisition and tracking linking controller.

Acknowledgments

The authors thank all of those involved in the Dynamic Compensation Experiment for all their long hours spent down at the site.

References

[1]Kalman, R. E., and Bucy, R., "New Results in Linear Filtering and Prediction," *Journal of Basic Engineering*, Vol. 83D, 1961, pp. 95–108.

[2]Benedict, T., and Bordner, G., "Synthesis of an Optimal Set of Radar Track-While-Scan Equations," *IEEE Transactions on Automatic Control*, Vol. AC-7, July 1962, pp. 27–32.

[3]Alspach, D. L., and Sorenson, H. W., "Nonlinear Bayesian Estimation Using Gaussian Sum Approximations," *IEEE Transactions on Automatic Control*, Vol. AC-17, No. 4, 1972, pp. 439–448.

[4]Chong, C. Y., Garren, D., and Greyson, T., "Ground Target Tracking—A Historical Perspective," *Proceedings of the IEEE Aerospace Conference*, Vol. 3, IEEE Press, New York, 2000, pp. 443–448.

[5]Lee, J. S., Ko, J. H., and Kim, E. S., "Real-Time Stereo Object Tracking System Using Block Matching Algorithm and Optical Binary Phase Extension Joint Transform Correlator," *Optical Communications*, Vol. 191, Nos. 3–6, 2001, pp. 191–202.

[6]Cusumano, S. J., Higgs, C., Tipton, C., and Jordan, D., "Active Tracking at Optical Wavelengths Through a Long Atmospheric Path," *IEEE Proceedings of the 36th Conference on Decision and Control*, Vol. 5, IEEE Press, New York, 1997, pp. 4949–4954.

[7]Haker, S., Sapiro, G., Tannenbaum, A., and Washburn, D., "Missile Tracking Using Knowledge-Based Adaptive Thresholding," *IEEE International Conference on Image Processing*, Vol. 1, IEEE Press, New York, 2001, pp. 786–789.

[8]Robertson, L., Johnson, C., Tipton, C., Jordan, D., Van Berg, C., Cleaver, A., and Manning, W., "Acquisition, Tracking and Pointing Hardware Architecture for the Non-Cooperative Dynamic Compensation Experiment," *Proceedings of the SPIE*, Vol. 4376, edited by W. E. Thompson and P. H. Merritt, Society of Photo-Optical Instrumentation Engineers, Bellingham, WA, 2001, pp. 57–68.

[9]Gelb, A., *Applied Optimal Estimation*, MIT Press, Cambridge, MA, 1992, p. 6.

[10]Roggeman, M., and Welsh, B., *Imaging Through Turbulence*, CRC Press, Boca Raton, FL, 1996, p. 70.

[11]Tyson, Robert, K., *Introduction to Adaptive Optics*, Society of Photo-Optical Instrumentation Engineers, Bellingham, WA, 2000, p. 7.

[12]"System Identification," MATLAB® Toolbox, Mathworks, Natick, MA.